

Updates to Pulsator Periods in NGC 3201

Avni Bansal
Paul Hamrick
Kalée Tock

Stanford Online High School, 415 Broadway Academy Hall, Floor 2, 8853, Redwood City, CA 94063; avnibansal2004@gmail.com; paulahamrick@gmail.com; kaleeg@stanford.edu

Received July 1, 2021; revised February 9, March 7, 2022; accepted March 7, 2022

Abstract The periods for RR Lyrae variables in NGC 3201 were calculated using the “string length method” in order to update or verify their periods. We confirm the published periods for 54 RR Lyraes in the cluster and offer eight period updates. We also identify the possibility that there is a non-linear CCD brightness response across different telescope cameras of the same specifications, which can result in pseudo-pulsations when multiple telescopes are used to image the cluster. Finally, we observe that in cases where two stars are very close together, source extractor photometry often only discerns one of the stars. Although point spread function photometry is more likely to discern both, it introduces challenges in identifying which star is which. The use of both photometric algorithms in tandem can help to untangle ambiguities.

1. Introduction

1.1. Pulsators

Pulsators are stars that periodically expand and contract in the process of maintaining hydrostatic equilibrium. Two classes of variables, RR Lyraes, and Cepheids, are used as standard candles for measuring large distances because their pulsation period and luminosity are related (Dall’Ora *et al.* 2006). For Cepheids, the period-luminosity relationship is pronounced and occurs across multiple wavelengths. For RR Lyraes, the period-luminosity relationship is more subtle and metallicity-dependent and occurs primarily at infrared wavelengths (Lee 1992). With those caveats, once the period of such a variable is known, its luminosity is also known. The luminosity can be compared to the apparent brightness to determine the pulsator’s distance.

In addition to improving distance measurements, accurate pulsator period measurements improve theoretical period-metallicity relationships in globular clusters. This is especially relevant to RR Lyrae stars as discussed above. Because period-luminosity-metallicity relationships are so important, we sought to independently calculate the periods of previously identified RR Lyrae stars in the globular cluster NGC 3201. The objective was to verify or update older period measurements.

1.2. Previous observations of NGC 3201

Periods for pulsators in NGC 3201 were first calculated in 1941 (Wright 1941). At that time, the cluster had 86 known pulsators. In that study, NGC 3201 was imaged using astronomical plates at the Boyden Station of Harvard Observatory near Arequipa, Peru. The periods were calculated manually from the plate data. The study succeeded in finding periods for all but 18 of the variables identified. These variables were either too close to other stars or had pulsation amplitudes too small to detect.

Since 1941, the search for new variables has continued in tandem with efforts to calculate ever more accurate periods for them. Initially, all analyses of NGC 3201 were photographic investigations. Photoelectric photometry such

as the investigation of 47 Tuc conducted at Siding Spring Observatory by Menzies (1973) became more common in the latter part of the century. A photoelectric photometer measures the brightness of a star based on the current produced when light falls onto a light-sensitive cathode. Every time a photon hits the cathode, an electric pulse is generated. The number of these signals per second indicates the star’s brightness, and using the frequency of pulses to measure brightness is known as pulse-counting photometry. Photographic data must undergo significant processing for brightnesses to be determined, while photoelectric photometry directly measures variations in brightness, so photoelectric methods soon replaced photographic methods as the standard measurement technique. For NGC 3201, the upgrade from photographic methods to photoelectric methods led to the discovery of nine new variables (Lee 1992).

As CCDs became more common, more discoveries were made about the stars of NGC 3201. Piersimoni *et al.* developed a model for the differential reddening of NGC 3201 in 2002 (Piersimoni *et al.* 2002), which was refined by Kravtsov *et al.* in 2009 (Kravtsov *et al.* 2009). CCDs led to the discovery of the first SX Phoenicis variables in NGC 3201, which are both dimmer and have lower amplitude pulsations than RR Lyrae stars (Mazur *et al.* 2003). Furthermore, some of the variables identified in the pre-CCD era were shown to be non-variable through CCD studies.

Layden and Sarjedini (2003) conducted the most comprehensive search for RR Lyraes in NGC 3201 to date. They searched for pulsators in their time-series BVI photometry data using three independent methods: the string length method, Lomb-Scargle, and their own template-finding method. The latter method entailed studying older light curves to make templates with the characteristic shapes of RR Lyraes and then fitting observed data points to these templates.

The periods of the 160 currently-known variables in NGC 3201 are listed in the Clement catalog (Clement *et al.* 2001). Using the catalog’s naming convention, the periods for stars V1 to V100 mostly come from Layden and Sarjedini (2003). They found reliable periods for most variables, with a

few exceptions. V6, V12, V19, V20, V27-V30, V36, and V45 either had uncertain phases, uncertain periods, or had too few or no data points at their minimum or maximum brightness. In addition, V8, V10, V37, V38, V51, and V76 were suspected of having the Blazhko effect. The Blazhko effect refers to periodic variations in the amplitude and phase of pulsation observed in RR Lyraes. The cause of the Blazhko effect is unclear, although several theories have been proposed (Smolec and Moskalik 2012).

A later study in 2014 (Arellano Ferro *et al.* 2014) used independently collected data as well as Layden and Sarajedini data to confirm the periods of V8, V12, V28, V36-V38, V45, and V76. They also confirmed that V28 was a Blazhko, and identified V18, V25, V50, and V73 as Blazkhos as well. V101-V143 are either SX Phoenicis (SXP), Beta-Lyrae type Eclipsing binaries (EB), or Algol type Eclipsing binaries (EA). It is currently uncertain whether V144-V160 are variables, and if so, what their classification is.

Since NGC 3201 is known to have some stars that exhibit the Blazhko effect, studying the periods of the stars over time can help to refine models of Blazhko period and amplitude changes over time. Furthermore, frequent recalculation of the period makes possible the identification of new Blazkhos. This is one of the reasons we have chosen to recalculate the periods of variables in NGC 3201. In addition, this study can improve the certainty in periods of variables whose periods we confirm.

1.3. Period-finding algorithm

This study uses a string-length method (Dworetzky 1983) algorithm that has been implemented by the authors. The period-finding method used here is an example of methods collectively known as Phase Dispersion Minimization (PDM), which reduces the range of values at a given phase of the light curve by minimizing a “cost function” of their scatter. VanderPlas (2018) gives a summary of several other commonly-used algorithms for characterizing periodicity in unevenly-sampled time-series data, including Fourier methods, phase-folding, least-squares, and Bayesian approaches. However, any of these would necessitate feeding the time-series data into an existing “black-box” PYTHON module. Also, the most commonly used of these methods, Lomb-Scargle, is optimized for sinusoidal data sets, and RR Lyrae pulsations are not sinusoidal in shape (VanderPlas 2018). Because PDM is conceptually straightforward enough to code ourselves from scratch, because it is well-suited to periodic data of any type, and because using it did not necessitate purchasing auxiliary software, it was chosen for this project. Details of our implementation are discussed further in section 2.5.

2. Procedure

2.1. Target selection

The globular cluster NGC 3201 was selected for three reasons. Firstly, it has several RR Lyraes with known periods, so we were able to compare our period estimates with previous ones. Secondly, NGC 3201 was visible while images for this study were being collected (February and March 2021). Lastly,

a majority of its RR Lyrae stars have an apparent magnitude lower than magnitude 17, so the 0.4-m telescopes of the Las Cumbres Observatory were able to image them clearly.

2.2. Instruments used

The instruments used were the Las Cumbres Observatory (LCO) telescopes in Cerro Tololo, Chile, in Siding Spring, Australia, in Sutherland, South Africa, and in Fort Davis, Texas (Brown *et al.* 2013). Each telescope has identical specifications, being 0.4 meter in aperture with a Meade 16-inch (40-cm) tube and three-element optics, mounted in LCO equatorial C-ring mounting. The optics are a primary, secondary, and Corrector plate (Meade) with an LCO focus mechanism driving corrector plate/secondary. The instruments on the telescopes also have identical specifications. The cameras are SBIG STL6303, which have a $19.5' \times 29.5'$ field of view and a pixel scale of 0.591. The images were taken with two of the eight filters provided by the Las Cumbres Observatory: Bessel-V and SDSS-ip, where SDSS stands for Sloan Digital Sky Survey (SDSS; Blanton *et al.* 2017). The Bessel V images were taken with an exposure time of 240 seconds and the SDSS-ip images were taken with an exposure time of 150 seconds. Images were taken through both filters at each epoch.

2.3. Image reduction

First, NGC 3201 was imaged in the V and ip filters. Images were taken with a cadence of approximately 3 hours between February 19 and February 27, 2021, and March 16 and March 23, 2021. Each image was plate solved and calibrated by LCO’s BANZAI pipeline. BANZAI calibration involves subtraction of a master dark multiplied by the corresponding image exposure time and then divided by a master flat. The full calibration procedure is described in McCully *et al.* (2018). Following this, the images were fed to the Our Solar Siblings (OSS) pipeline, which transformed their original Julian Date timestamps to Barycentric Julian dates, computed from the latitude, longitude, elevation of the corresponding LCO telescope, along with the R.A. and Dec. of the target. The OSS pipeline performed six different photometric extraction algorithms on the images (Fitzgerald 2018). Of these six, the Point Spread eXtractor (psx) and Source Extractor (sex) photometries were used (Bertin and Arnouts 1996). Psx was used because it is a point spread function fitting photometry (Hamrick *et al.* 2021). Point spread function fitting photometry can be effective at pinpointing the magnitudes of stars in crowded fields such as that of NGC 3201 (Heasley 1999). Sex photometry was used because using two different photometric algorithms lowers the likelihood of being misled by blended pairs.

2.4. Reference star selection

After photometric reduction, reference stars were chosen. Initially, a list of reference stars was generated using the autocal function, which is part of the astrosources python module (Fitzgerald *et al.* 2021). One reference among those identified by the software was selected, and all the known pulsators in NGC 3201 were then calibrated against it. However, when we calculated periods using stars that were calibrated in this way, we found that a large fraction of periods

were close to one day or half a day. This was puzzling for two reasons. Firstly, older period estimates for the RR Lyraes in NGC 3201 range from 0.1 to 0.6 day instead of being concentrated around half a day or a day. Secondly, it is highly unlikely that most of the RR Lyraes in NGC 3201 have periods of such similar fractions of a day.

The similarity of the periods suggested the following hypothesis: the periodicity may be an aliasing effect, arising as an artifact of which Las Cumbres Observatory telescope is being used at different times during the night. For example, if the target is the highest for the telescope in Tenerife around 9 P.M. UTC but highest for Texas around 6 A.M. UTC, then most of the early evening observations will be taken in Tenerife while most of the late evening–early morning (UTC) observations will be taken in Texas.

Although the reference star we had used to calibrate magnitudes is meant to control for different imaging circumstances, if the reference is much brighter or dimmer than the target, then non-linearity in the camera’s response to photons might come into play. Specifically, consider the example where the reference star is much brighter than the target, and the Tenerife camera responds to that difference in a slightly different way than the Texas camera does, despite the identical specifications of the two instruments. In this case, we might see a pseudo-pulsation which is an artifact of which camera took the images rather than a pulsation of the star itself, and the period of the pseudo-pulsation would be close to 1 day or a multiple thereof.

To control for this, we selected multiple reference stars based on several criteria. First, each reference star had to appear in the Gaia and APASS catalogs (Gaia Collab. 2016, 2018; Henden *et al.* 2016). Second, the calibrated magnitude of each reference star had to have a standard deviation of less than 0.03 magnitude with respect to at least five check stars across the entire image series. Finally, the reference star had to appear in every time-series image photometry file. One criterion that we chose not to factor in was the color of the reference star since the differential CCD response of the instruments used was based on magnitude only. In addition to this, the color of an RR Lyrae star often changes as it pulsates, making the best color reference star tricky to pin down.

Once the reference stars that met these criteria were identified, each known pulsator was calibrated against the reference star that was closest to it in magnitude. Because the magnitudes of the target and pulsator were near-identical, the differential brightness response of the cameras was no longer a factor. This careful selection of reference stars successfully eliminated the pseudo-pulsations with periods of half a day or a day. The nonlinearity was reported to LCO and was traced by the LCO science team to a differential accumulation of dust on the optics between instruments. The reference stars identified for psx photometry, V-filter images are shown in Figure 1. These include two of the AAVSO-recommended comparison stars shown in Figure 2 and Table 1: 000-BPD-811 and 000-BPD-812.

2.5. Period-finding using string length

We wrote PYTHON code, which we will call “GENIE,” to calculate the pulsation periods. GENIE takes each star’s time-

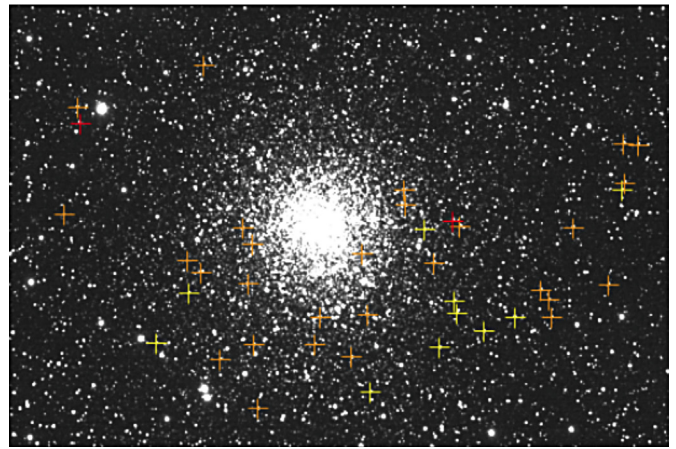


Figure 1. Reference stars found in psx V filter, labeled with colors corresponding to spectral type. Red stars have APASS B–V magnitudes greater than 1.3, orange stars have APASS B–V magnitudes between 0.9 and 1.3, and yellow stars have APASS B–V magnitudes between 0.3 and 0.9 (APASS; Henden *et al.* 2016).

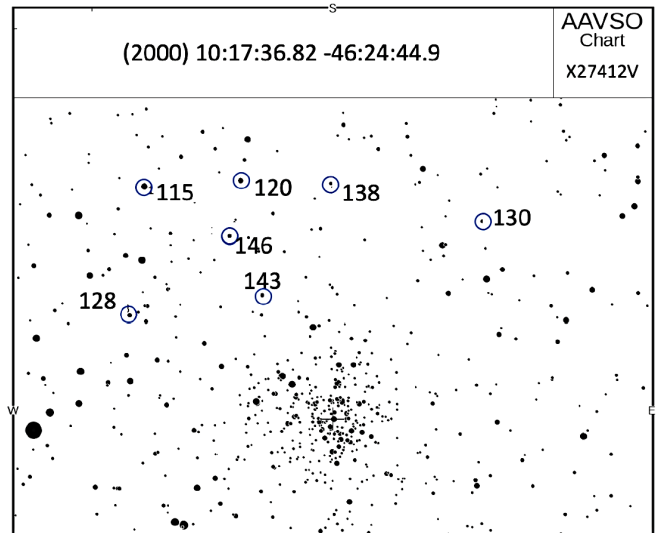


Figure 2. AAVSO recommended comparison stars from the Variable Star Plotter, chart X27412V. Of these, the stars labeled 138 and 143 (AUID 000-BPD-811 and AUID 000-BPD-812) were also identified as appropriate reference stars within our data set according to the criteria outlined above. See Table 1.

Table 1. AAVSO recommended comparison stars from the Variable Star Plotter, chart X27412V (shown in Figure 2).

AUID	R.A. (°)	Dec. (°)	Label	V	B–V
Epoch 2021-02-01 (2021.08767)–2021-03-23 (2021.22466)					
000-BPD-807	154.18971	–46.59292	115	11.483	0.559
000-BPD-808	154.29900	–46.59750	120	12.017	0.593
000-BPD-809	154.17329	–46.49244	128	12.833	0.771
000-BPD-810	154.57425	–46.56581	130	12.993	0.930
000-BPD-811	154.40138	–46.59531	138	13.760	0.009
000-BPD-812	154.31262	–46.51139	143	14.261	0.706
000-BPD-813	154.28625	–46.55450	146	14.575	0.824

Note: Of these, the stars labeled 138 and 143 (AUID 000-BPD-811 and AUID 000-BPD-812) were also identified as appropriate reference stars within our data set according to the criteria outlined above.

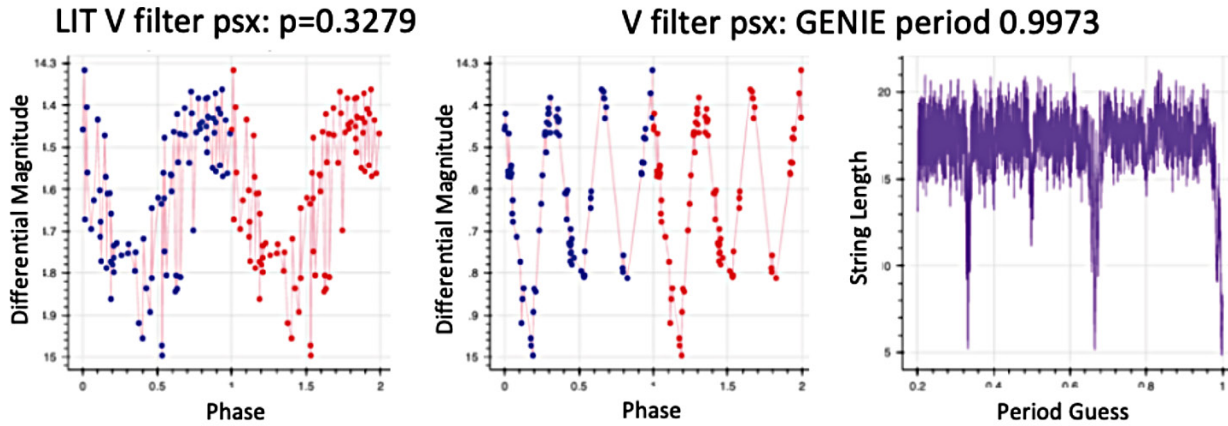


Figure 3. V67, or ASASSN-V J101700.89-462635.3: two phases of the light curve folded over the literature period (left), two phases of the light curve folded over the GENIE period (center), and the corresponding string-length plot (right).

series photometry data in the V and ip filters and folds them over periods ranging from 0.1 to 1 day, at 0.001-day increments. For each fold, a “string length” is computed for the plot of magnitude versus time (Dworetzky 1983). The string length is defined as follows: if one were to take a string and overlay it on the light curve, the string length is the length of that string on the graph. The shortest string length will correspond to the “smoothest” or most continuous light curve. Thus, whichever period yielded the shortest string length became our period estimate/GENIE period.

A plot of string length versus period is analogous to an inverted power spectrum. Manual analysis of these plots helped to catch cases where the string length was deceptive. For example, if the string length plot showed multiple minima, corresponding to harmonic oscillations, then the best period identified by the code might be a multiple of the true period. Alternatively, if the string length plot did not show a clear minimum, then it is unlikely that the brightness plot would show a clear pulsation when folded over the code-identified period.

After determining the GENIE period, light curves were plotted by folding over both the literature period and the GENIE period. Upon examination of the light curves, we visually determined which period between the GENIE period and the literature period yielded a clearer pulsation pattern. Because of the idiomatic nature of this test, estimating the error of the period presents difficulties. One technique involves taking the width of the string length plot 5% or 50% of the way up from its minimum value (Altunin *et al.* 2020; VanderPlas 2018). However, this technique is problematic because the noise in the string length plot makes the position of the plot’s baseline difficult to pin down, and further ambiguity is introduced by the local minima that occur near multiples or fractions of the correct period. Therefore, a conservative estimate is to assign error bars to our GENIE periods whose width encompasses the corresponding literature period for the star.

3. Results

3.1. Nomenclature of the stars

The stars are referred to by their Clement catalog names, augmented where available by their AUIDs, and their listings

in the ASAS-SN catalog, WISE catalog, and WASP catalog (Jayasinghe *et al.* 2021; Greer *et al.* 2017; Wright *et al.* 2010; Clement *et al.* 2001).

3.2. Periods found

One limitation of most period-finding methods is that multiples and fractions of the actual period (harmonics) also fit the data quite well. This is because folding the light curve over multiples of the actual period also yields a relatively clean curve. In some cases, the string length of the light curve folded over a multiple of the actual period may be slightly shorter than that of the actual period. An example of this is shown in Figure 3.

In Figure 3, all three multiples of the pulsator’s period are represented by minima of approximately the same depth in the string length plot at right. However, visual confirmation of multiple pulses in the light curve invalidates the longer periods. Period-finding methods may sometimes identify multiples of the correct period, as ours did for this system, because any behavior that is periodic over a time x is also periodic over whole number multiples of x .

Another initial anomaly in the first run of the GENIE code was that a large proportion of pulsators apparently had periods of close to a day or half a day. As discussed in section 2, Procedure, the artificial pulsation was likely induced by a non-linear CCD brightness response across different LCO cameras. Thus GENIE initially found that 28% of pulsators seemed to have a period over 0.9 day. After reference stars were selected as described above and filtered for similarity in brightness to each pulsator target, the artificial pulsations went away. This suggests that our rigorous reference star selection procedure reduced the likelihood that the reference was significantly brighter or dimmer than its corresponding target.

After making these corrections, the known RR Lyrae pulsators in the cluster became clearly evident, and their light curves are shown in Appendix A. In addition, we identified eight pulsators for which the GENIE period yielded significantly cleaner light curves than the literature period did. These are tabulated in Table 2 and shown in Figure 4. The literature periods and pulsator classes quoted in Table 1 were taken from the Clement catalog (Clement *et al.* 2001). This catalog cited Layden and Sarajedini (2003) as the source for the literature periods.

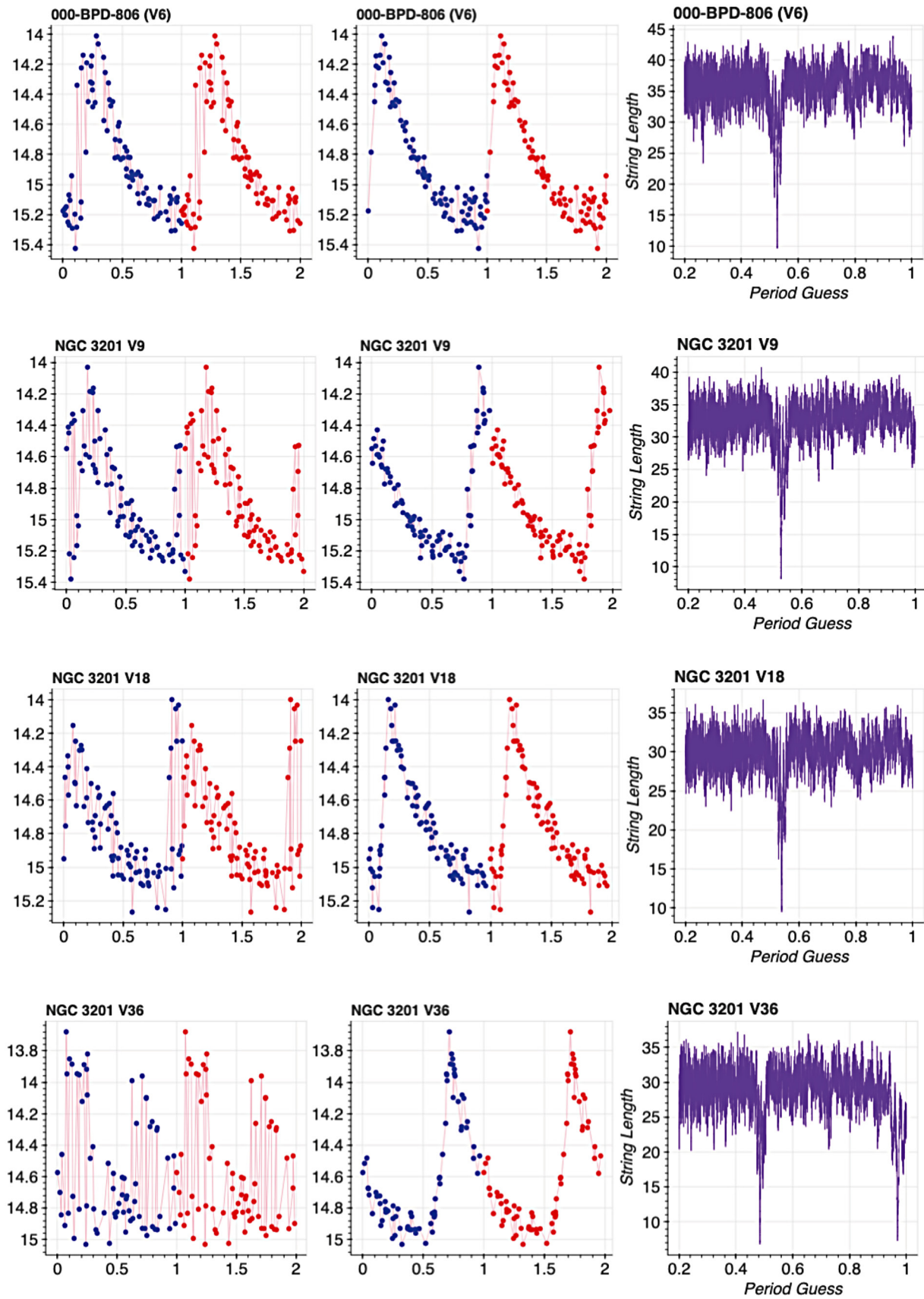


Figure 4. Left: Calibrated magnitude versus phase folded over the literature period from Table 1. Middle: Calibrated magnitude versus phases folded over the GENIE period from Table 1. Right: String length plot. (Figure continued on next page.)

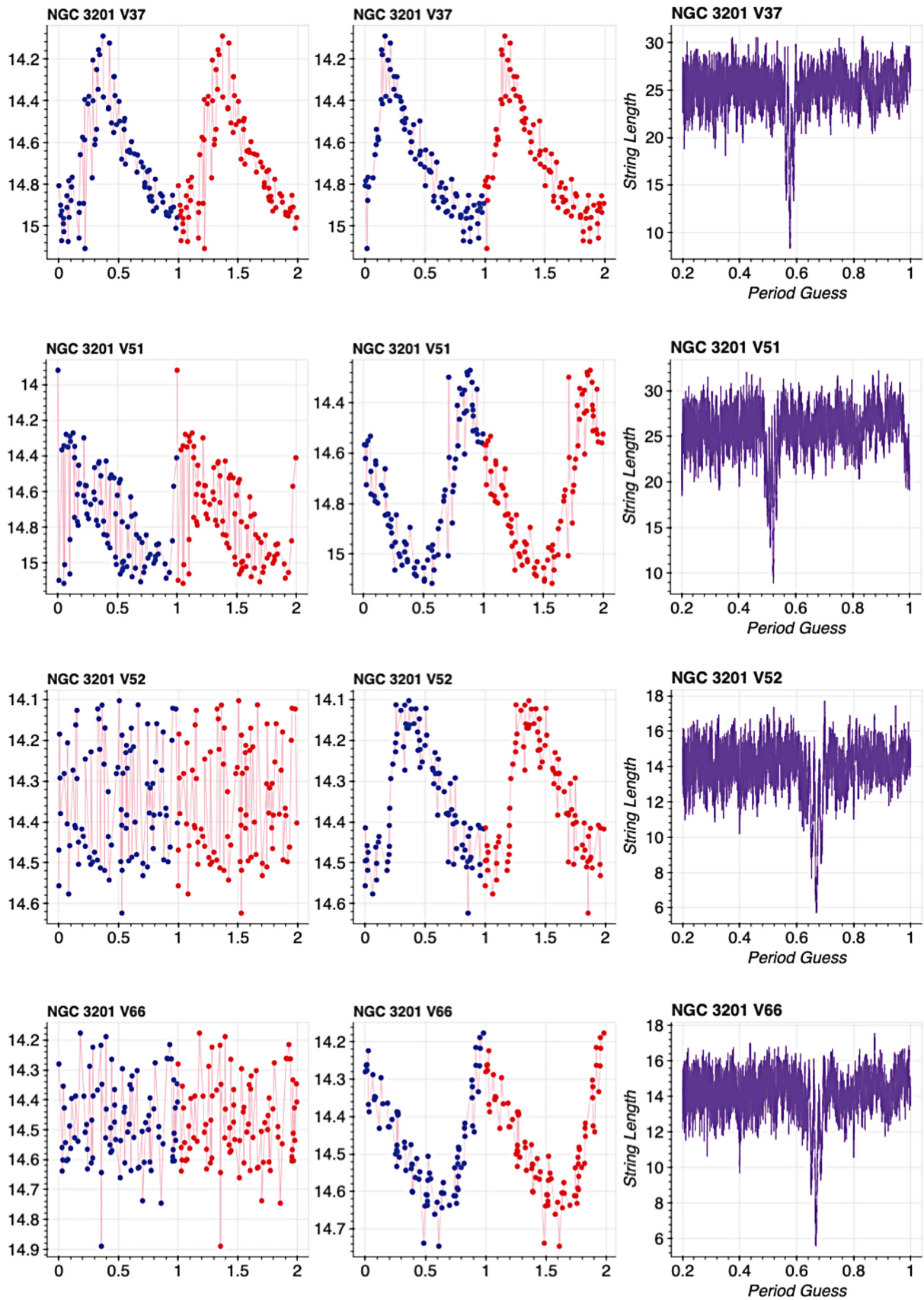


Figure 4 (cont.). Left: Calibrated magnitude versus phase folded over the literature period from Table 1. Middle: Calibrated magnitude versus phases folded over the GENIE period from Table 1. Right: String length plot.

Table 2. The position, class, literature period, and GENIE period for updated pulsators.

<i>Clement Catalog Name</i>	<i>R.A. (°)</i>	<i>Dec. (°)</i>	<i>Clement Catalog Pulsator Class</i>	<i>GENIE Period</i>	<i>Layden (2003) Period</i>
<i>Epoch 2021-02-01 (2021.08767)–2021-03-23 (2021.22466)</i>					
000–BPD–806 (NGC 3201 V6)	154.35875	–46.45063	RR0	0.5263	0.5253
NGC 3201 V9	154.38457	–46.43683	RR0	0.5271	0.5254
NGC 3201 V18	154.41408	–46.41839	RR0	0.5389	0.5404
NGC 3201 V36	154.36265	–46.41464	RR0	0.4844	0.4796
NGC 3201 V37	154.37793	–46.43212	RR0	0.5766	0.5751
NGC 3201 V51	154.32363	–46.41839	RR0	0.5214	0.5186
NGC 3201 V52	154.40958	–46.63284	RR1	0.6691	0.38
NGC 3201 V66	154.24627	–46.33007	RR2	0.6675	0.284

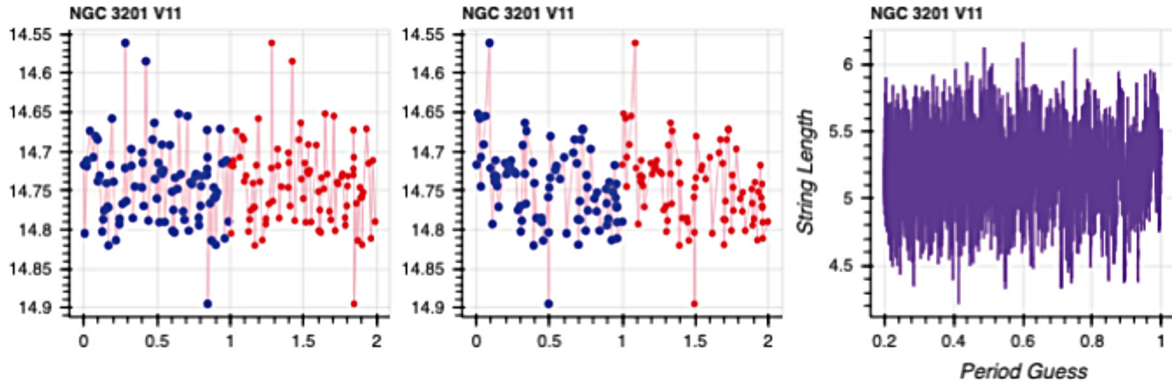


Figure 5. NGC 3201 V11. Left: Calibrated magnitude versus phase folded over the literature period from Table 1. Middle: Calibrated magnitude versus phases folded over the GENIE period from Table 1. Right: String length plot.

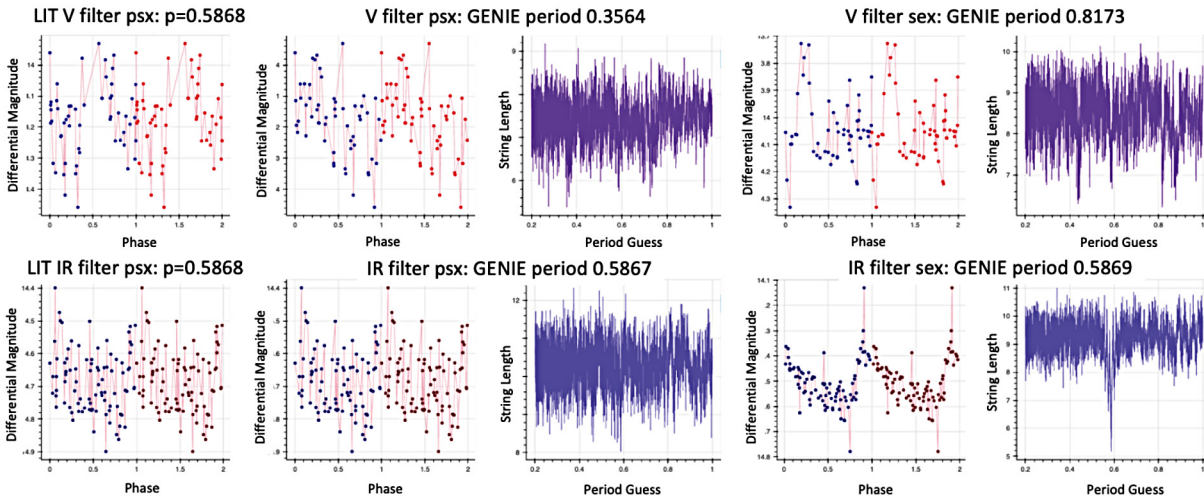


Figure 6. NGC 3201 V23, pulsator for which only the sex IP light curve is clearly pulsing.

Table 3. Photometry file for psx V photometry file (Bertin and Arnouts 1996), with three stars very close together.

<i>R.A. (°)</i>	<i>Dec. (°)</i>	<i>Pixel X</i>	<i>Pixel Y</i>	<i>ADU Count X</i>	<i>ADU Count Y</i>	<i>Error X</i>	<i>Error Y</i>
<i>Epoch 2021-02-01 (2021.08767)–2021-03-23 (2021.22466)</i>							
154.3863432	–46.4291925	1602.9081	927.7031	41177.74	316.8156	7.614074 ⁻⁶	3.741641 ⁻⁶
154.3803840	–46.4232605	1565.3450	901.5863	40363.49	315.9283	6.314095 ⁻⁶	3.153824 ⁻⁶
154.3860066	–46.4255095	1579.5896	926.3909	90200.72	392.6851	3.316372 ⁻⁶	3.998483 ⁻⁶

In each case, a visual comparison was made between the light curve folded over the literature period and the light curve folded over the GENIE period for both V and ip filters, in both psx and sex photometry. For simplicity, we display the literature and GENIE period for only V filter, psx photometry in the plots of Figure 4. Note that the last two light curves represent RR Lyrae stars of type RR1 and RR2, respectively, according to their Clement catalog classifications. They have a pulse profile with a correspondingly different shape than the sharp sawtooth light curve characteristic of an RR0.

The discrepancies between the GENIE period and literature periods in Table 1 have unclear origins. Typical changes in RR Lyrae periods are on the scale of 0.2 or 0.5 day every one million years, but the changes found here are significantly more. However, previous articles have found much greater discrepancies than predicted as well (Neilson *et al.* 2016). The reason for these discrepancies is presently unknown. We note that the most drastic differences (V52 and V66) correspond to stars for which no amplitude or magnitude is listed in the Clement catalog and that V6 and V36 were stars for which Layden and Sarajedini did not find reliable periods, as discussed previously. Also of note is the fact that V18 is one of the stars highlighted in the introduction as a suspected Blazhko (Arellano Ferro *et al.* 2014).

Analogous plots to those shown in Figure 4 were also generated for psx photometry in the ip filter, sex photometry in the V filter, and sex photometry in the ip filter. The GENIE periods were almost or exactly identical to those found above, and the GENIE period light curves compared similarly to the literature period light curves as for psx photometry in the V filter. Therefore, these 72 additional plots are not shown.

The fact that GENIE found the same period as the literature value for 50 of the stars in Appendix A, and that folding over the GENIE period sharpens and smooths the light curves in Figure 4, improves confidence in the string-length period-finding method. For V52 and V66, although the GENIE period is much larger than the literature period by almost a full multiple, we are confident that the GENIE period is valid because there is only one dip in the string length plot and the light curve shows a clear pulse. However, it should be noted that these stars are type RR1 and RR2 rather than RR0. RR1s and RR2s typically have shorter periods of about 0.3 day. Hence the GENIE period of approximately double that is surprising. Further investigation may reveal that these stars should be reclassified, possibly to RR0s.

In addition to offering some updates, we also draw attention to some special cases. For the NGC 3201 V11 pulsator, neither the GENIE period nor the literature period yielded a light curve that appeared to be pulsing, as shown in Figure 5. We hypothesize that this star may have been incorrectly identified in our images. In this case, the plots below may pertain to an entirely different star.

Another special case is NGC 3201 V23, for which pulsation was only evident in the sex ip-filter light curve. This is shown in Figure 6.

One hypothesis is that in some filters and photometries, stars that are close together are being blended. As shown in Table 3, there are three stars with an R.A. starting with 154.38

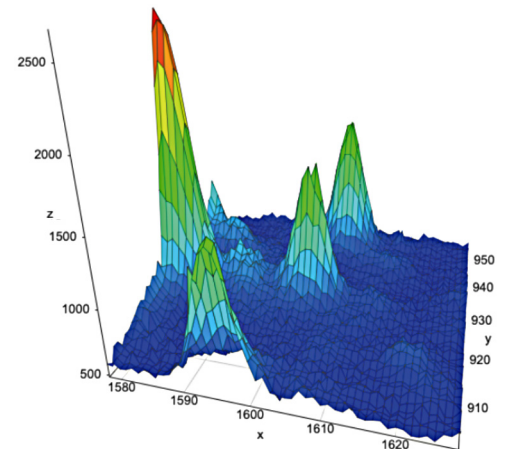
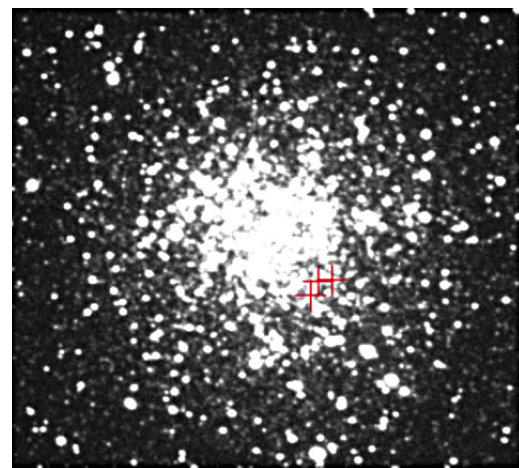


Figure 7. Region surrounding the three stars highlighted in Table 3, as seen on the image (top) and as a surface in three dimensions (bottom).

and Dec. starting with -46.42 in the psx V photometry. Figure 7 shows this region of the crowded starfield, along with a surface plot of ADU count as a function of x and y pixel coordinates. Since the stars are so close together, it can be challenging to pick out which star is which. GENIE's criterion was to find the closest star to the Gaia coordinates relative to the image plate solution within 2 arcseconds, which may be inadequate. If the incorrect star is identified as the pulsator in some images, the pulse may be obscured.

The figures above imply that sex V may be showing one of the non-pulsators while sex ip shows the pulsator. When stars are very close together, sex photometry likely finds either the brightest one only or a blend of multiple stars. Perhaps the non-pulsator is brighter in the V filter, but the pulsator is brighter in the ip filter.

Another item to note is that our methods failed to find accurate periods for SX Phoenicis (SXP) pulsators. Although some of our SXP light curves show some evidence of pulsation when folded over the literature period, there is no sharp dip in the string length plots. This is likely because the SXP pulsators are very dim, having magnitudes close to 17, which is near the limit of what the Las Cumbres 0.4-m telescopes can observe. Secondly, SXPs usually have pulsations of less than 0.3 magnitude (Aerts 2010). Thus the SXP pulse often does not rise above the noise floor for our images, and the string length

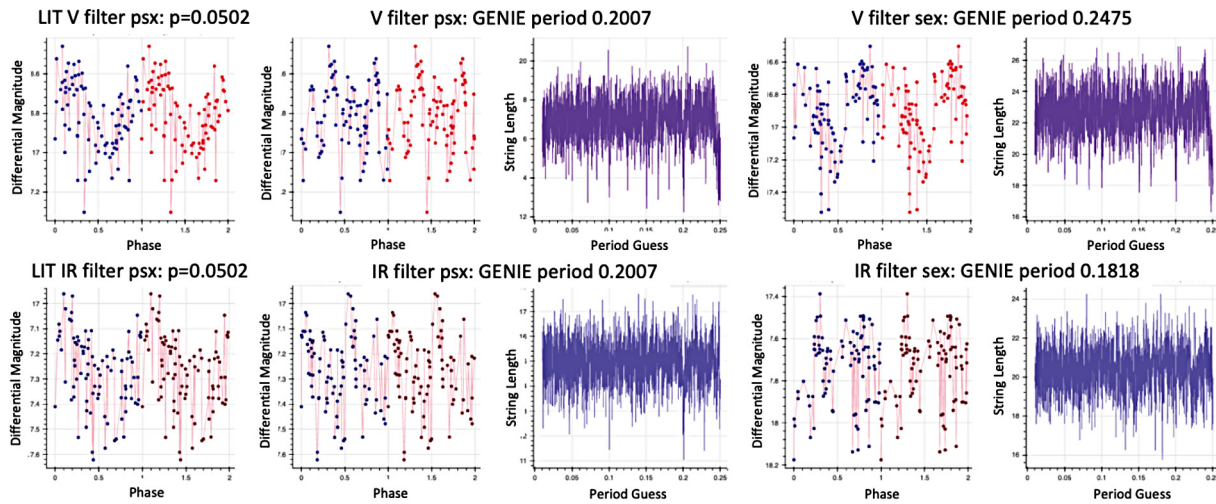


Figure 8. Light curves and string length plot for SXP pulsator NGC 3201 V110.

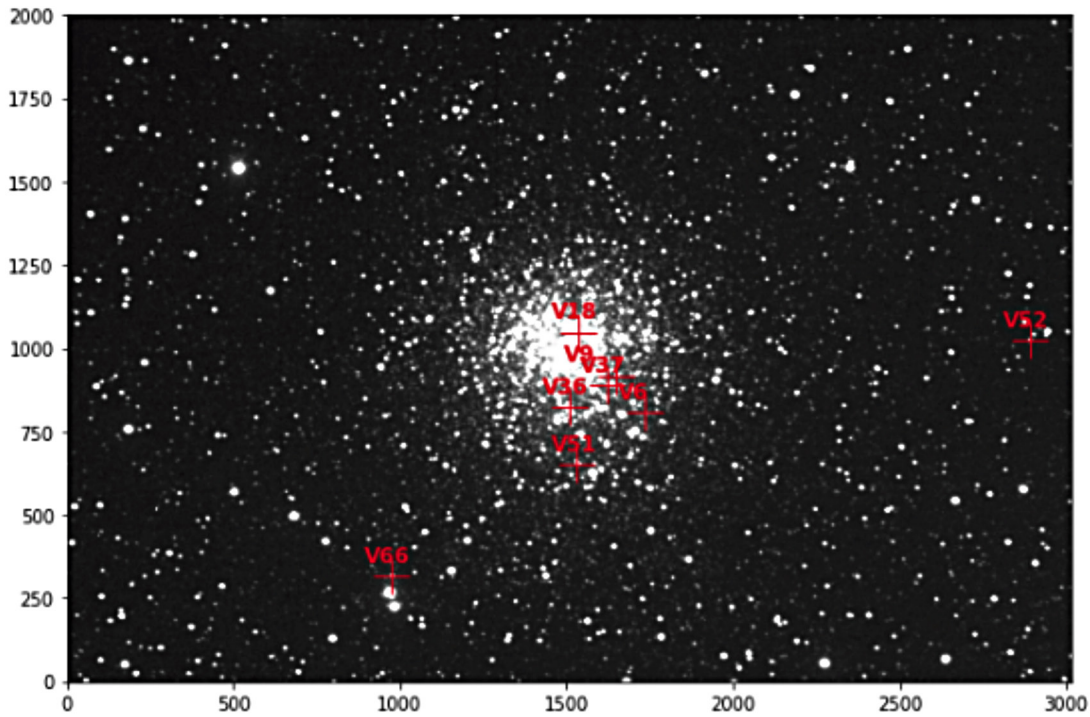


Figure 9. The pulsators whose periods are updated by this study include NGC 3201 V6 (000-BPD-806), V9, V18, V36, V37, V51, V52, and V66.

method may not be appropriate for such cases. When folded over the literature period, we did see evidence of one SXP pulsation, shown in the plots for NGC 3201 V110 in Figure 8. The literature period and classification as an SXP for V110 were also obtained from the Clement catalog (Clement *et al.* 2001). The Clement catalog cites Mazur *et al.* (2003) as the source for this pulsator's period.

3.3. Distribution of data and results

Sharing data with the scientific community makes more extensive studies possible. The AAVSO maintains several databases for the purpose of facilitating the storing and sharing of data pertinent to variable stars. At present, these databases are set up to tie each observation to a particular observing site, which

is problematic for the LCO Global Telescope network. Although the 0.4-m LCO telescopes have identical specifications, they are located at multiple sites all over the world. It is not possible to submit observations taken by multiple telescopes within the same data file being uploaded via WebObs to the AAVSO International Database, and separating the observations by telescope is impractical given the large number of images in this study. That said, the images and photometry are all freely accessible on Google Drive from the links in Appendix A, or by corresponding with the study authors.

The authors are exploring uploading the photometry to the AAVSO International Database.

4. Conclusions

Our GENIE code for finding periods using the string-length method appears to be sound. 54 of the periods of pulsators in NGC 3201 were confirmed, and the periods of the eight pulsators highlighted above were updated. The positions within the cluster of the stars whose period updates are presented are shown in Figure 9.

Secondly, we caution that a non-linear CCD brightness response across different cameras is possible, even when these cameras have the same specifications. This can result in pseudo-pulsations. However, this can be overcome by ensuring that the reference and the pulsator stars are of near-identical brightness.

Thirdly, we point out that using two or more different photometries minimizes the chances of being misled by blended stars, because at least one of the photometries may be able to isolate close stars instead of blending them.

5. Acknowledgements

This work makes use of observations taken by the 0.4-m telescopes of Las Cumbres Observatory Global Telescope Network located in Cerro Tololo, Chile, in Siding Spring, Australia, in Sutherland, South Africa, and in Fort Davis, Texas, reduced using the Our Solar Siblings Pipeline. This research was made possible through the use of the AAVSO Photometric All-Sky Survey (APASS), funded by the Robert Martin Ayers Sciences Fund, and the International Variable Star Index, maintained by the AAVSO.

The authors would particularly like to thank Daniel Zaharevitz for his PYTHON coding help, as he was the original author of a script that we adapted to visualize the positions of particular stars within the cluster. We would also like to thank Chuck Cynamon for his assistance in generating an AAVSO sequence for the NGC 3201 field, and requesting AUIDs for many of our targets. In addition, Michael Fitzgerald was an invaluable source of help and advice, especially regarding the operation of the LCO telescopes and the possible nonlinearity of the CCD sensor.

References

- Aerts, C., Christensen-Dalsgaard, J., and Kurtz, D. W. 2010, *Asteroseismology*, Springer Science+Business Media B.V., Berlin (DOI: 10.1007/978-1-4020-5803-5).
- Altunin, I., Caputo, R., and Tock, K. 2020, *Astron. Theory Obs. Methods*, **1**, 1 (DOI: 10.32374/atom.2020.1.1).
- Arellano Ferro, A., Ahumada, J. A., Calderón, J. H., and Kains, N. 2014, *Rev. Mex. Astron. Astrofis.*, **50**, 3 (arXiv:1406.2635).
- Bertin, E., and Arnouts, S. 1996, *Astron. Astrophys., Suppl. Ser.*, **117**, 393 (DOI: 10.1051/aas:1996164).
- Blanton, M. R., et al. 2017, *Astron. J.*, **154**, 28 (Sloan Digital Sky Survey IV, <https://www.sdss.org/>).
- Brown, T. M., et al. 2013, *Publ. Astron. Soc. Pacific*, **125**, 1031 (DOI: 10.1086/673168).
- Clement, C. M., et al. 2001, *Astron. J.*, **122**, 2587 (DOI: 10.1086/323719).
- Dall’Ora, M., et al. 2006, *Mem. Soc. Astron. Ital.*, **77**, 214 (arXiv:astro-ph/0601237).
- Dworetzky, M. M. 1983, *Mon. Not. Roy. Astron. Soc.*, **203**, 917 (DOI: 10.1093/mnras/203.4.917).
- Fitzgerald, M. 2018, *Robotic Telesc. Student Res. Education Proc.*, **1**, 347 (DOI: 10.32374/rtstre.2017.033).
- Fitzgerald, M., Gomez, E., Salimpour, S., Singleton, J., and Wibowo, R. 2021, *J. Open Source Software*, **6**, 2641 (DOI: 10.21105/joss.02641).
- Gaia Collaboration, et al. 2016, *Astron. Astrophys.*, **595A**, 1.
- Gaia Collaboration, et al. 2018, *Astron. Astrophys.*, **616A**, 1.
- Greer, P. A., Payne, S. G., Norton, A. J., Maxted, P. F. L., Smalley, B., West, R. G., Wheatley, P. J., and Kolb, U. C. 2017, *Astron. Astrophys.*, **607A**, 11 (DOI: 10.1051/0004-6361/201630296).
- Hamrick, P., Bansal, A., and Tock, K. 2021, *J. Amer. Assoc. Var. Star Obs.*, **49**, 192.
- Heasley, J. N. 1999, in *Precision CCD Photometry*, eds. E. R. Craine, D. L. Crawford, R. A. Tucker, ASP Conf. Ser. 189, Astronomical Society of the Pacific, San Francisco, 56.
- Henden, A. A., Templeton, M., Terrell, D., Smith, T. C., Levine, S., and Welch, D. 2016, *VizieR Online Data Catalog: AAVSO Photometric All Sky Survey (APASS) DR9*, II/336.
- Jayasinghe, T., et al. 2021, *Mon. Not. Roy. Astron. Soc.*, **503**, 200. (DOI: 10.1093/mnras/stab114).
- Kravtsov, V., Alcaíno, G., Marconi, G., and Alvarado, F. 2009, *Astron. Astrophys.*, **497**, 371 (DOI: 10.1051/0004-6361/200810555).
- Layden, A. C., and Sarajedini, A. 2003, *Astron. J.*, **125**, 208 (DOI: 10.1086/344948).
- Lee, Y.-W. 1992, *Mem. Soc. Astron. Ital.*, **63**, 331.
- Mazur, B., Krzemiński, W., and Thompson, I. B. 2003, *Mon. Not. Roy. Astron. Soc.*, **340**, 1205.
- McCully, C., Volgenau, N. H., Harbeck, D.-R., Lister, T. A., Saunders, E. S., Turner M. L., Siiverd, R. J., and Bowman, M. 2018, *Proc. SPIE*, id. 107070K (<https://arxiv.org/pdf/1811.04163.pdf>).
- Menzies, J. 1973, *Mon. Not. Roy. Astron. Soc.*, **163**, 323 (DOI: 10.1093/mnras/163.3.323).
- Neilson, H. R., Percy, J. R., and Smith, H. A. 2016, *J. Amer. Assoc. Var. Star Obs.*, **44**, 179.
- Piersimoni, A. M., Bono, G., and Ripepi, V. 2002, *Astron. J.*, **124**, 1528.
- Smolec, R., and Moskalik, P. 2012, *Mon. Not. Roy. Astron. Soc.*, **426**, 108 (DOI: 10.1111/j.1365-2966.2012.21678.x).
- VanderPlas, J. T. 2018, *Astrophys. J., Suppl. Ser.*, **236**, 16 (DOI: 10.3847/1538-4365/aab766).
- Wright, F. W. 1941, *Bull. Harvard Coll. Obs.*, No. 915, 2.
- Wright, E. L., et al. 2010, *Astron. J.*, **140**, 1868. (DOI: 10.1088/0004-6256/140/6/1868).

Appendix A

We confirm the periods of the 54 RR Lyrae pulsators in NGC 3201, listed by their Clements Catalog variable names in Table A1 and shown in Figure A1. These include 50 stars for which GENIE code found a period less than 0.001 day different from the literature value. In addition, we include one star (NGC 3201 V80) whose light curve folded over the literature period (0.5887 day) was cleaner than when folded over the GENIE period (0.5901 day), and one star (NGC 3201 V76) for which neither the literature period nor the GENIE period was decidedly cleaner. Finally, we include two stars for which folding over the literature period produced a clean light curve but GENIE found a multiple of the period. These are NGC 3201 V16 (ASASSN-V J101718.47-462836.5) and NGC 3201 V67 (ASASSN-V J101700.89-462635.3). Thus, in total, we confirm the periods of 54 stars.

Three of the stars in this “confirmed” list are suspected Blazhko stars: NGC 3201 V25 (ASASSN-V J101746.15-462152.1), NGC 3201 V28, and NGC 3201 V73 (ASASSN-V J101725.20-462315.1). These are noted in Table A1.

A list of stars that were not positively identified in at least 50 of our images of the cluster is shown in Table A2. Stars that were outside the field of view of our images are noted.

Links to the original images along with the OSS photometry appear in Table A3.

In Table A4, all 64 of the RR Lyrae stars identified in our images are listed by their Clements Catalog names and alternative designations where available. Of these, 54 of the periods were confirmed (Table A1), eight of the periods were updated (Main Study Table 1), and two of the stars did not display a clear pulse (V11 and V23, shown in Main Study Figures 5 and 6).

Table A1. NGC 3201 stars whose periods are confirmed by this study, with suspected Blazhko stars indicated.

NGC 3201 Star		
1	25 Blazhko susp.	47
2	26	48
3	27	49
4	28 Blazhko susp.	55
5	29	56
7	30	57
8	31	58
10	32	59
13	34	67
14	35	71
15	38	73 Blazhko susp.
16	39	76
17	40	78
19	41	80
20	42	83
21	43	84
22	44	98
24	46	100

Table A2. NGC 3201 stars that were not positively identified in the images for this study, which suspected Blazhko stars and stars that were outside the image FOV indicated.

NGC 3201 Star			
12		77	
33		79	
45		81	
50	Blazhko susp.	82	
53–54	Outside FOV	85–89	Outside FOV
60–64	Outside FOV	90	
65		91	Outside FOV
68–69	Outside FOV	92	
70		93–96	Outside FOV
72		97	
74		99	
75			

Table A3. Repository of images and photometry used for this study.

<i>Available through Google Drive</i>		
Images		https://tinyurl.com/NGC3201images
Photometry	V psx	https://tinyurl.com/NGC3201Vpsx
	V sex	https://tinyurl.com/NGC3201Vsex
	ip psx	https://tinyurl.com/NGC3201ipsex
	ip sex	https://tinyurl.com/NGC3201isex
<i>Available through the AAVSO ftp public datasets site (photometry only)</i>		
ftp://ftp.aavso.org/public/datasets/J50.1-Bansal-NGC3201/small_phot_files-20220329T185408Z-001.zip		
ftp://ftp.aavso.org/public/datasets/J50.1-Bansal-NGC3201/NGC3201_sex_V-20220329T185526Z-001.zip		
ftp://ftp.aavso.org/public/datasets/J50.1-Bansal-NGC3201/NGC3201_psx_ip-20220329T185836Z-001.zip		
ftp://ftp.aavso.org/public/datasets/J50.1-Bansal-NGC3201/NGC3201_sex_ip-20220329T190205Z-001.zip		

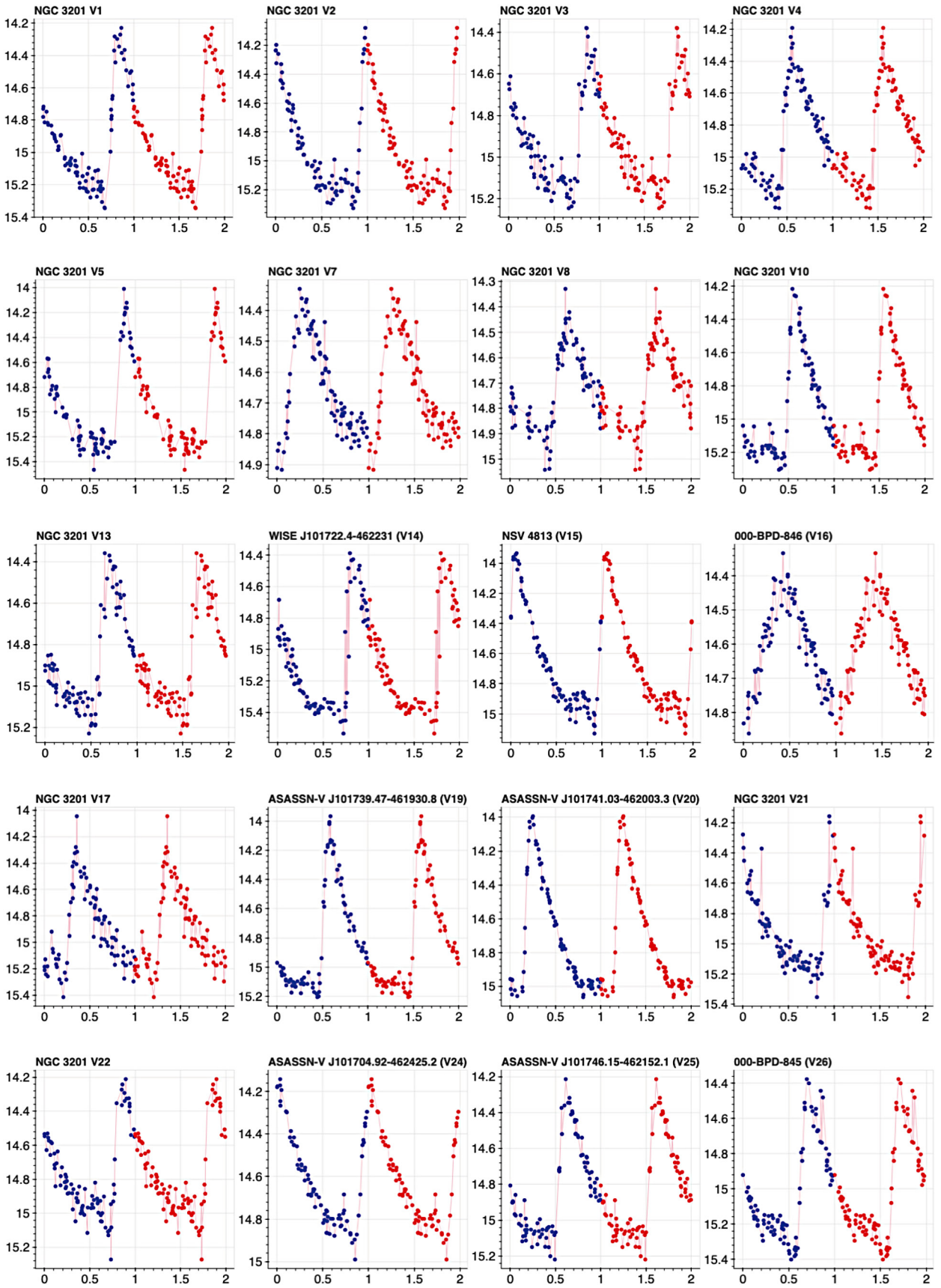


Figure A1. Light curves of 54 RR Lyrae variable stars whose literature periods are confirmed by this study. (Figure continued on following pages.)

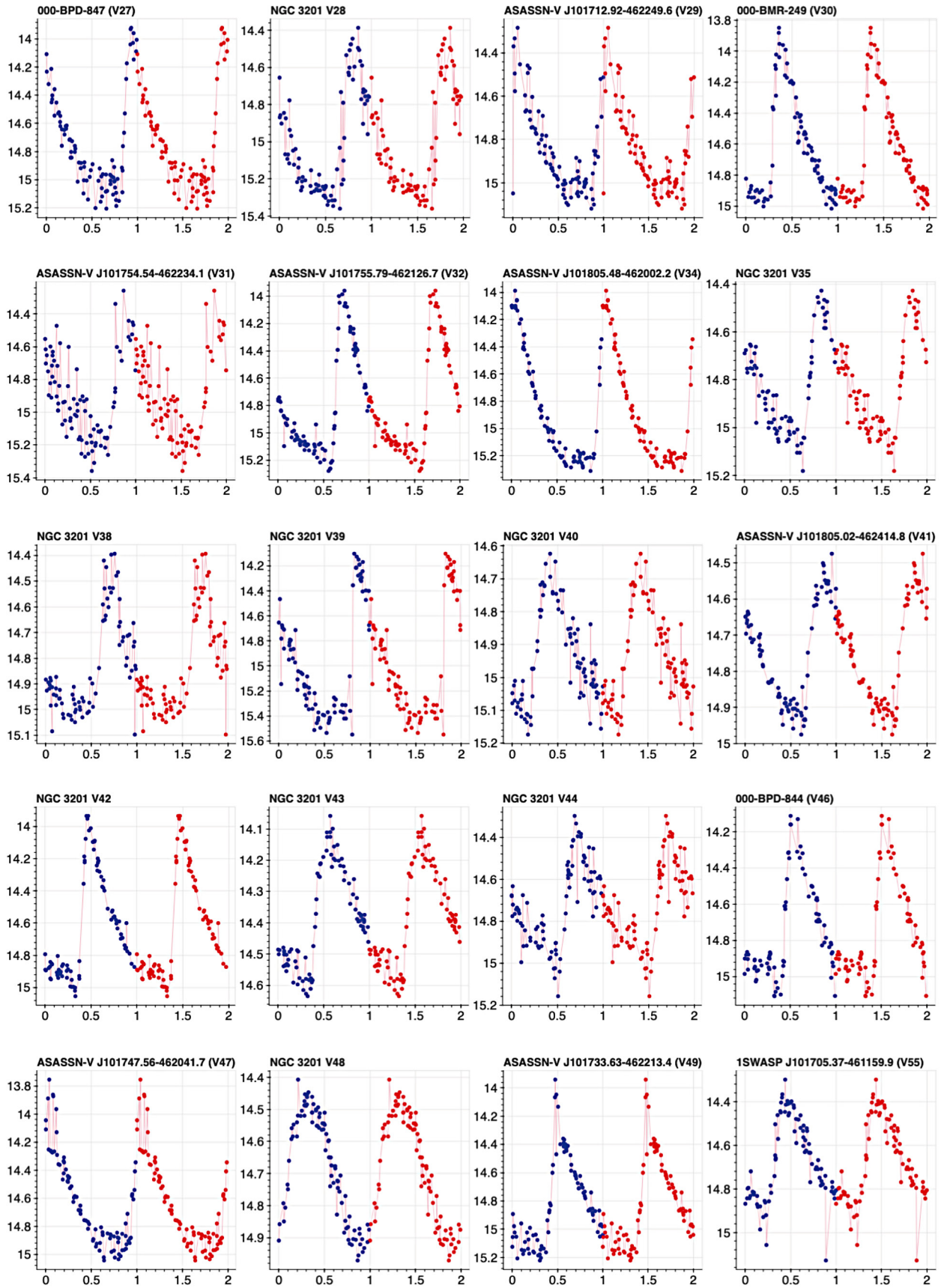


Figure A1. Light curves of 54 RR Lyrae variable stars whose literature periods are confirmed by this study (cont.). (Figure continued on next page.)

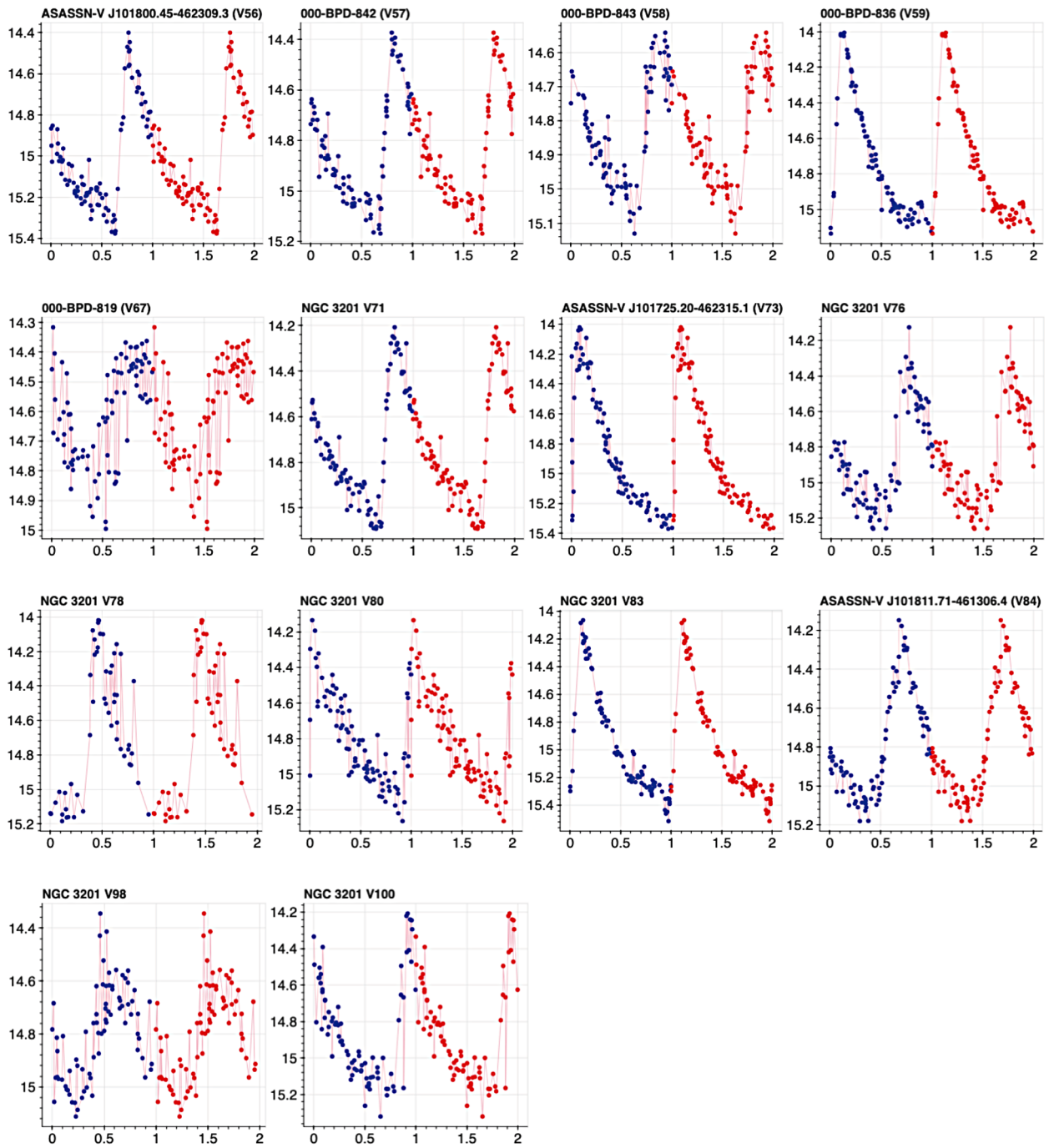


Figure A1. Light curves of 54 RR Lyrae variable stars whose literature periods are confirmed by this study (cont.).

Table A4. All 64 of the RR Lyrae stars identified in the images of this study.

Number	Name	AUID	R.A. (°)	Dec. (°)	Type	Publ. Mag.	Publ. Ampl.	Publ. Period	Genie Best Period	Notes
<i>Epoch 2021-02-01 (2021.08767)–2021-03-23 (2021.22466)</i>										
1	NGC 3201 V1	000-BPD-806	154.42844	−46.44382	RR0	14.81	0.92	0.6048	0.6049	
2	NGC 3201 V2		154.41666	−46.44385	RR0	14.8	1.07	0.5326	0.5327	
3	NGC 3201 V3		154.47705	−46.42376	RR0	14.91	0.8	0.5994	0.5993	
4	NGC 3201 V4		154.46677	−46.41124	RR0	14.8	1.02	0.63	0.6303	
5	NGC 3201 V5		154.42208	−46.41844	RR0	14.73	0.94	0.5013	0.5011	
6	ASASSN-V J101726.09-462702.3		154.35875	−46.45063	RR0	14.74	0.9	0.5253	0.5263	updated in this study
7	NGC 3201 V7		154.36872	−46.46352	RR0	14.69	0.67	0.6303	0.6301	
8	NGC 3201 V8		154.37817	−46.4387	RR0	14.74	0.73	0.6286	0.6286	
9	NGC 3201 V9		154.38457	−46.43683	RR0	14.82	0.96	0.5254	0.5271	updated in this study
10	NGC 3201 V10		154.33394	−46.34726	RR0	14.84	0.88	0.5352	0.5352	
11	NGC 3201 V11		154.36483	−46.38211	RR1	14.79	0.58	0.2991	0.4146	no clear pulse
13	NGC 3201 V13		154.34185	−46.38644	RR0	14.85	0.88	0.5748	0.5753	
14	WISE J101722.4-462231		154.34349	−46.3754	RR0	14.99	1.13	0.5089	0.5093	
16	ASASSN-V J101718.47-462836.5	000-BPD-846	154.327	−46.47683	RR1	14.62	0.63	0.2634	0.5269	multiple pulses
17	NGC 3201 V17		154.40963	−46.41867	RR0	14.76	0.92	0.5658	0.5655	
18	NGC 3201 V18		154.41408	−46.41839	RR0	14.74	1.05	0.5404	0.5389	Blazhko, updated in this study
19	ASASSN-V J101739.47-461930.8		154.4145	−46.32524	RR0	14.73	0.92	0.525	0.5251	
20	ASASSN-V J101741.03-462003.3		154.42092	−46.33431	RR0	14.68	1.07	0.5291	0.5289	
21	NGC 3201 V021		154.44267	−46.37483	RR0	14.83	0.73	0.5668	0.5667	
22	NGC 3201 V22		154.36528	−46.42723	RR0	14.75	0.86	0.6058	0.606	
23	NGC 3201 V23		154.38604	−46.42521	RR0	14.8	0.77	0.5868	0.3564	no clear pulse
24	ASASSN-V J101704.92-462425.2		154.27053	−46.40702	RR0	14.65	0.76	0.589	0.5889	
25	ASASSN-V J101746.15-462152.1		154.44235	−46.36448	RR0	14.73	1.05	0.5147	0.5145	Blazhko
26	ASASSN-V J101758.09-462701.8	000-BPD-845	154.49208	−46.45049	RR0	14.91	0.92	0.569	0.569	
27	ASASSN-V J101742.79-463001.0	000-BPD-847	154.42842	−46.50035	RR0	14.76	1.21	0.4843	0.4843	
28	NGC 3201 V28		154.43131	−46.42512	RR0	14.87	0.86	0.5795	0.5786	Blazhko
29	ASASSN-V J101712.92-462249.6		154.30387	−46.38046	RR0	14.78	0.68	0.5291	0.5298	
30	NGC 3201 V30	000-BMR-249	154.29131	−46.33731	RR0	14.6	0.87	0.5159	0.5161	
31	ASASSN-V J101754.54-462234.1		154.47734	−46.37615	RR0	14.9	1.26	0.5191	0.5191	
32	ASASSN-V J101755.79-462126.7		154.48248	−46.35742	RR0	14.73	1.24	0.5612	0.5611	
34	ASASSN-V J101805.48-462002.2		154.52289	−46.33397	RR0	14.75	1.27	0.4679	0.4679	
35	NGC 3201 V35		154.40129	−46.37867	RR0	14.75	0.63	0.6155	0.6156	
36	NGC 3201 V36		154.36265	−46.41464	RR0	14.73	1.26	0.4796	0.4844	updated in this study
37	NGC 3201 V37		154.37793	−46.43212	RR0	14.74	1.05	0.5751	0.5766	updated in this study
38	NGC 3201 V38		154.38092	−46.42806	RR0	14.81	0.81	0.5094	0.5093	
39	NGC 3201 V39		154.42186	−46.39713	RR0	14.81	1.2	0.4829	0.4833	
40	NGC 3201 V40		154.36674	−46.3933	RR0	14.84	0.58	0.6437	0.644	
41	ASASSN-V J101805.02-462414.8		154.52097	−46.40411	RR0	14.81	0.45	0.665	0.6648	
42	NGC 3201 V42		154.28616	−46.3578	RR0	14.61	1.22	0.5382	0.5381	
43	NGC 3201 V43		154.25569	−46.40719	RR0	14.65	0.5	0.6761	0.6765	
44	NGC 3201 V44		154.41703	−46.39355	RR0	14.76	0.62	0.6107	0.6106	
46	1SWASP J101657.56-463212.1	000-BMR-249	154.24628	−46.55113	RR0	14.74	0.98	0.5432	0.5432	
47	ASASSN-V J101747.56-462041.7		154.44823	−46.34493	RR0	14.65	0.89	0.5212	0.521	
48	NGC 3201 V48		154.3056	−46.408	RR1	14.68	0.65	0.3413	0.3413	
49	ASASSN-V J101733.63-462213.4		154.39018	−46.3704	RR0	14.72	1.04	0.581	0.5813	
51	NGC 3201 V51		154.32363	−46.41839	RR0	14.72	1.16	0.5186	0.5214	updated in this study
52	NGC 3201 V52		154.40958	−46.63284	RR1	—	—	0.38	0.6691	updated in this study
55	1SWASP J101705.37-461159.9		154.27246	−46.20005	RR0	14.57	0.55	0.6041	0.6048	
56	ASASSN-V J101800.45-462309.3		154.50307	−46.38613	RR0	14.89	0.79	0.5903	0.5905	
57	ASASSN-V J101804.87-462554.6	000-BPD-842	154.52035	−46.43183	RR0	14.83	0.71	0.5934	0.5935	
58	ASASSN-V J101810.58-462604.6	000-BPD-843	154.54413	−46.43462	RR0	14.7	0.72	0.622	0.6229	
59	1SWASP J101651.71-462523.2	000-BPD-836	154.20851	−46.43049	RR0	14.66	1.08	0.5177	0.5179	
66	NGC 3201 V66	000-BPD-819	154.24627	−46.33007	RR2	—	—	0.284	0.6675	updated in this study
67	ASASSN-V J101700.89-462635.3		154.25376	−46.44314	RR1	14.69	0.39	0.3279	0.9973	multiple pulses
71	NGC 3201 V71		154.3307	−46.44347	RR0	14.7	0.78	0.6012	0.6013	
73	ASASSN-V J101725.20-462315.1		154.35504	−46.38753	RR0	14.76	1.24	0.5195	0.5199	Blazhko
76	NGC 3201 V76		154.38039	−46.42321	RR0	14.81	0.66	0.5267	0.5254	
78	NGC 3201 V78		154.40374	−46.45109	RR0	14.85	1	0.5139	0.5137	
80	NGC 3201 V80		154.4295	−46.40467	RR0	14.8	0.59	0.5887	0.5901	* see note
83	NGC 3201 V83		154.47821	−46.36511	RR0	14.78	1.23	0.5452	0.5452	
84	ASASSN-V J101811.71-461306.4		154.54879	−46.2185	RR0	14.8	0.94	0.5137	0.5137	
98	NGC 3201 V98		154.35666	−46.42184	RR1	14.78	0.43	0.3363	0.3356	
100	NGC 3201 V100		154.40067	−46.4078	RR0	14.77	1.02	0.5485	0.5489	

* GENIE period different but light curve not cleaner.